Temperature evolution of the relaxor dynamics in $Pb(Zn_{1/3}Nb_{2/3})O_3$: A critical Raman analysis

J. Toulouse,* F. Jiang,† and O. Svitelskiy‡
Department of Physics, Lehigh University, Bethlehem, Pennsylvania 18015, USA

W. Chen and Z.-G. Ye
Department of Chemistry, Simon Fraser University, Vancouver, British Columbia, Canada V58 1S6
(Received 4 August 2004; revised manuscript received 26 July 2005; published 22 November 2005)

At the heart of the relaxor behavior lies the development of mesoscopic or intermediate range order and the low frequency or relaxation dynamics associated with it. To investigate this development, we have measured the Raman spectra of a $Pb(Zn_{1/3}Nb_{2/3})O_3$ (PZN) single crystal over a wide temperature range from 1000 K to 150 K. The spectra are analyzed using several different physical models, focusing particularly on the low frequency part. Both relaxation and coupled phonon dynamics are identified. The evolution of the relaxor dynamics is marked by three characteristic temperatures, Burns temperature, $T_B \simeq 650$ K, and two other temperatures, $T_d \simeq 470$ K and $T_f \simeq 340$ K, which together define four major ranges. Combining the fitting results from the Raman spectra and other experimental results in PZN, we describe the relaxor dynamics in these four ranges, in terms of the strength and lifetime of the correlations between off-center ions. Relating the dynamics observed in PZN to that in $KTa_{1-x}Nb_xO_3$ (KTN), we develop a microscopic model based on the coexistence of a fast and a slow motion of the off-center Pb and Nb ions which accounts for both types of dynamics (coupled phonon and relaxational) between T_B and T_f, and show evidence for a series of local phase transitions taking place below T_d.

DOI: 10.1103/PhysRevB.72.184106 PACS number(s): 77.84.Dy, 78.30.−j, 67.80.Cx, 77.22.Gm

I. INTRODUCTION

Relaxor ferroelectrics $A(B'B'')O_3$ have been studied extensively in the past several years because of their important technical applications and original fundamental physics.[1–4] They are characterized by the mixed occupancy of the B site and the off-centering of some of the ions. In $Pb(Zn_{1/3}Nb_{2/3})O_3$ (PZN), the B site can be occupied by either niobium or zinc and in $Pb(Mg_{1/3}Nb_{2/3})O_3$ (PMN) by either niobium or magnesium. Differences in the atomic radii and valences of the two B-site cations can lead to the formation of chemically ordered regions with a $Fm\bar{3}m$ space symmetry dispersed in a disordered matrix with an average $Pm\bar{3}m$ space symmetry.[5–7] The other essential characteristics of relaxors is the presence of off-center ions imparting electric dipole moments to individual unit cells. In lead relaxors, the Pb ions have clearly been shown to be displaced from their high symmetry site, although the direction of the displacement is not definite for all of them. ($\langle 111\rangle$, $\langle 110\rangle$, or spherical distribution). In PMN, x-ray results have suggested either $\langle 110\rangle$ displacements[8] or a spherical distribution,[9] particularly at high temperatures, also suggested by nuclear magnetic resonance (NMR) results.[10] In PZN, a Pb displacement in the $\langle 111\rangle$ direction seems more probable.[11] More recently, the Nb ions have also been shown to be displaced from their site in a $\langle 111\rangle$ direction, although by a smaller amount.[5,6,12,13] This is also the case in the nonlead relaxor $KTa_{1-x}Nb_xO_3$ (KTN).[14] As a result of symmetry, Pb^{2+} and Nb^{5+} can each occupy either 12 or eight equivalent off-center positions in the unit cell. At high temperature, both are expected to switch relatively freely between these positions and the time-averaged structure remains cubic.[9] At lower temperature, their positions and motions become correlated, giving rise to the formation of polar nanoregions (PNRs) and to their low frequency or relaxational dynamics. The structural aspects of the PNRs have been studied by x-ray,[15,16] neutron diffraction and elastic neutron scattering.[17–22] The development of a mesoscopic structural order in relaxors is now well documented and best identified by the appearance of diffuse elastic neutron scattering.[19,22] The wave vector width of the diffuse scattering peak Δq (in units of $2\pi/a$, with a being the lattice parameter), provides a direct measurement of the extent of the intermediate range order or correlation length, $\zeta = 2/\Delta q$, and the distribution of the diffuse scattering intensity in reciprocal space provides information on the internal structure and orientation of the PNRs.[22] The dynamical aspects of the PNRs have been studied using various spectroscopies, dielectric spectroscopy,[23–27] neutron scattering, and light scattering (Raman, Brillouin).[28–36] With regards to the relaxor dynamics, the frequency width $\Delta\omega$ of the central peak (CP) that appears in the inelastic light or neutron scattering spectra around zero energy provides a direct measurement of the characteristic relaxation time, $\tau = 2/\Delta\omega$. Raman scattering has the advantage that light couples directly to polarization and is therefore well suited for a study of the PNR dynamics. In addition, one can acquire the entire spectrum in one sweep, covering both relaxations at lower frequencies and vibrational excitations at higher frequencies. Moreover, because the wave vector conservation rule does not apply in disordered systems and all wave vectors can therefore contribute, Raman is well suited for the study of relaxors in which excitations on different length scales are coupled. On the other hand, this can also render the interpretation of the Raman spectra more difficult, which is one of the challenges addressed in the present paper.

The Raman spectra of relaxors would normally be expected to contain two characteristic features, a soft phonon

mode and a central peak (CP). However, these spectra have been difficult to interpret for three reasons. First, they exhibit broad and overlapping peaks, particularly in the low frequency region which contains the relaxor-relevant features. This suggests the existence of coupling between relaxation(s) and phonon excitations. Second, as mentioned above, the Raman spectra of relaxors can contain contributions from all possible wave vectors in the Brillouin zone and one needs to identify which wave vectors contribute within a given frequency range in order to understand the physics. Finally, photons can be scattered in both chemically ordered and disordered regions. For the preceding reasons, it is therefore necessary to assume a model and then fit the spectra accordingly, in order to separate the spectral features and identify their origins. A number of Raman studies of relaxor ferroelectrics have been reported.[28–33] However, in all these studies the authors may have oversimplified the problem by fitting their spectra using a single model and concluding to its validity on the basis of the goodness of fit. In the present paper, we report a more complete Raman study of PZN. We analyze the entire spectrum using several possible models and show that all of them give excellent fits to the spectra. Only through a cross-examination of the fitting results obtained with these different models are we able to evalulate the plausibility of each of them, identify the relevant physical mechanisms and understand their evolution with temperature: dynamical correlations between off-center ions, the appearance of the PNRs and their reorientational dynamics, coupling between relaxation and phonon excitations, local phase transitions and eventually freezing. The physical description that emerges from this analysis draws from this cross-examination, from complementary measurements made on PZN and from a comparison between KTN, PMN, and PZN. In a previous paper,[37] we analyzed the behavior of the CP in KTN, PMN, and PZN, and found striking similarities between the three compounds. In the present paper, we expand on this comparison and develop a general framework to describe the temperature evolution of the relaxor dynamics. An essential element of this framework is the existence of an intermediate temperature, which truly marks the appearance of permanent PNRs, often associated with Burns temperature in the past. For this reason, in the present paper, we choose to designate Burns temperature as T_B and use T_d for the intermediate temperature. The third and final temperature is the freezing temperature, T_f.

II. EXPERIMENT

The PZN crystal used in this study was grown by the high temperature solution technique. A rectangular slab sample was cut from a large as-grown crystal along ⟨100⟩, with dimensions $5\times5\times7$ mm^3. All faces were polished to an optical finish. The sample was excited by an argon ion laser with a wavelength of 514 nm and a power of 300 mW. A right-angle scattering geometry was used, in which the incident light was along x-⟨100⟩ and the scattered light was detected along y-⟨010⟩. Polarized spectra $x[zz]y$ (*VV*) and $x[zx]y$ (*VH*) were recorded over a wide temperature range while cooling from 1000 K to 150 K, using a double-grating ISA Jobin Yvon spectrometer equipped with a Hamamatsu photomultiplier R-649. For most of the measurements, the slits were opened to 1.7 cm^{-1}. However, at temperatures close to the maximum of the dielectric constant, the slits were narrowed down to 0.6 cm^{-1} in order to acquire more precise data in the low frequency or quasielastic region.

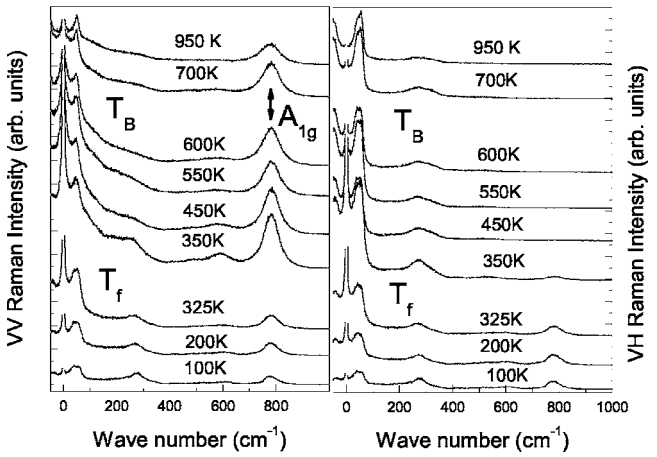

FIG. 1. Examples of Raman spectra taken at different temperatures for (a) $x(zz)y$ (*VV*) and (b) $x(zx)y$ (*VH*) upon cooling. x, y, and z are along cubic crystal axial directions and the phonon wave vector is along ⟨110⟩.

III. RESULTS

Figure 1 shows examples of *VV* and *VH* Raman spectra at different temperatures. The spectra have been separated into three groups from top to bottom: those above T_B, between T_B and T_f, and below T_f. It should be noted that the Raman spectra show marked changes around $T_f \simeq 340$ K and that T_f is well below the dielectric maximum temperature T_m, which is around 420 K.[38] The Raman spectra shown in Fig. 1 are typical of relaxors and are consistent with spectra reported in the literature. As mentioned in the Introduction, all modes are broad and overlapped, and no clear mode softening is observed. Consequently, a complete symmetry assignment of the Raman peaks is difficult. Nonetheless, based on a critical analysis of our Raman spectra and on other complementary experimental results (e.g., neutron scattering), definite modes and their mutual coupling can still be identified. In the next few sections we first make general remarks about these Raman spectra and then carry out a critical analysis using several physically plausible models.

A. Two-phase model and Raman mode assignment

Early evidence of short range chemical order on the B sublattice was reported in the form of weak diffuse $(h+1/2, k+1/2, l+1/2)$ superlattice reflection peaks in selected area electron diffraction (SAED).[39–41] The short range order was later confirmed by high resolution synchrotron x-ray diffraction, showing that chemical order is primarily responsible for the superlattice diffraction peaks.[42–45] Two models have been proposed for chemical ordering on the B sublattice: the space-charge model and the random layer (random site)

model.[7,39,44,46] Both models suggest an $Fm\bar{3}m$ space group for the chemically ordered regions. These ordered regions are dispersed in a disordered matrix with an average $Pm\bar{3}m$ space group. One should therefore expect the Raman spectra to be a superposition of two scattering contributions, one from the chemically ordered nanoregions and the other from the disordered matrix with average cubic symmetry $Pm\bar{3}m$.[47] Group theoretical analysis show that the vibrational modes for the two different phases are[48,49]

disordered matrix;

$$Pm\bar{3}m(Z=1) \quad \text{for } T > T_c,$$

$$3T_{1u}(\mathrm{IR}) + T_{2u}(I)$$

$$\downarrow$$

$$R3m(Z=1) \quad \text{for } T < T_c,$$

$$3A_1(\mathrm{IR},R) + 4E(\mathrm{IR},R) + A_2(I),$$

ordered nanoregions;

$$Fm\bar{3}m(Z=2) \quad \text{for } T > T_c,$$

$$A_{1g}(R) + E_g(R) + 2T_{2g}(R) + T_{1g}(I) + 4T_{1u}(\mathrm{IR}) + T_{2u}(I)$$

$$\downarrow$$

$$R3m(Z=2) \quad \text{for } T < T_c$$

$$7A_1(\mathrm{IR},R) + 2A_2(I) + 10E(\mathrm{IR},R),$$

where T_c is the presumed phase transition temperature. However, as we shall see below, there is no single T_c but a transition region. IR and R designate infrared and Raman active modes and I represents a silent mode. At very high temperatures, none of the modes are Raman active for the $Pm\bar{3}m$ phase, although Raman modes from the ordered regions of $Fm\bar{3}m$ can appear, $A_{1g}(R)+E_g(R)+2T_{2g}(R)$, all of which are nonpolar modes. The Raman tensors associated with these symmetry modes are

$$A_{1g}:\begin{pmatrix} a & & \\ & a & \\ & & \end{pmatrix}; \quad E_g:\begin{pmatrix} b & & \\ & b & \\ & & -2b \end{pmatrix};$$

$$T_{2g}:\begin{pmatrix} & d & \\ d & & d \\ & d & \end{pmatrix}.$$

The most clearly identifiable feature of the spectra is the mode around 780 cm^{-1}, which exhibits marked temperature and polarization dependencies. As shown in Fig. 2, this mode is also well separated from other modes in the high temperature cubic phase; it appears in the *VV* but not in the *VH* spectrum and has therefore been assigned an A_{1g} symmetry.[28,29,47] At low temperature, it appears in both the *VV* and the *VH* spectra due to symmetry lowering. An intense mode is also observed in the low frequency region of the spectrum at 50 cm^{-1}, which, in view of recent neutron scattering studies,[50,51] may represent a contribution from the flat zone boundary transverse acoustic mode, TA(ZB), made possible by the disorder. It is interesting to note that this 50 cm^{-1} peak is a singlet in *VV* but a doublet in *VH* at high temperatures, and a doublet in both *VV* and *VH* below T_f (this is more clearly seen in PMN).[31] If one of the components of the doublet most likely represents the contribution from the zone boundary transverse acoustic mode, the other may either arise from a splitting of the former upon symmetry lowering or, alternatively, from the T_{2g} mode in the chemically ordered regions. At intermediate frequencies, a shoulder composed of at least two strongly overlapping peaks is visible between 75 cm^{-1} and 150 cm^{-1}. It too exhibits a marked polarization dependence; at 350 K and above, it appears in the *VV* but not in the *VH* spectrum. It most likely contains a contribution from the TO_1 mode in the disordered regions. This assignment is supported by neutron scattering, which reveal a broad or highly damped result that show a broad or highly damped TO_1 mode on the high frequency side of the TA(ZB), eventually disappearing below T_B ("waterfall" phenomenon). The other contribution is unclear at this point. For this reason, and because it would be difficult to obtain reliable sets of parameters for two separate modes, we chose to fit the shoulder with a single peak. In this way, reliable physical parameters can be obtained for the central peak and the other low frequency modes, even though the TO frequency thus obtained is most likely too high. At T_f, the intensity in this part of the *VV* spectrum is drastically reduced with the loss of the shoulder between 75 cm^{-1} and 150 cm^{-1}, and a sharp decrease in intensity and splitting of the 50 cm^{-1} peak. The characteristically different polarized

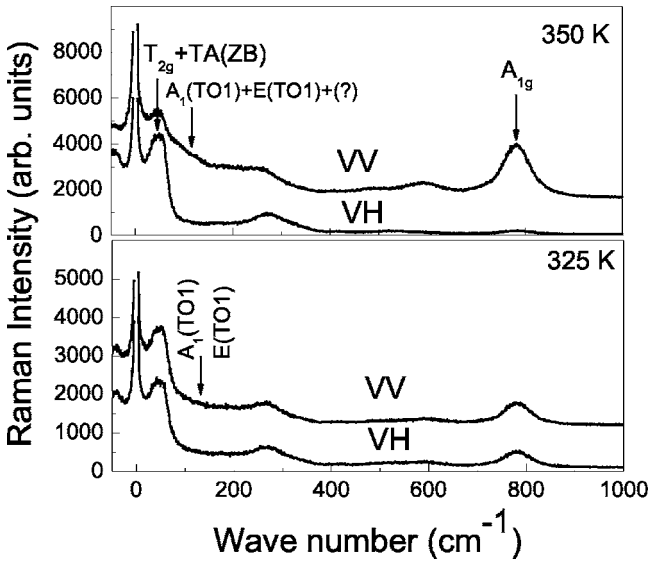

FIG. 2. Polarization dependence of the Raman spectra just below and above T_f.

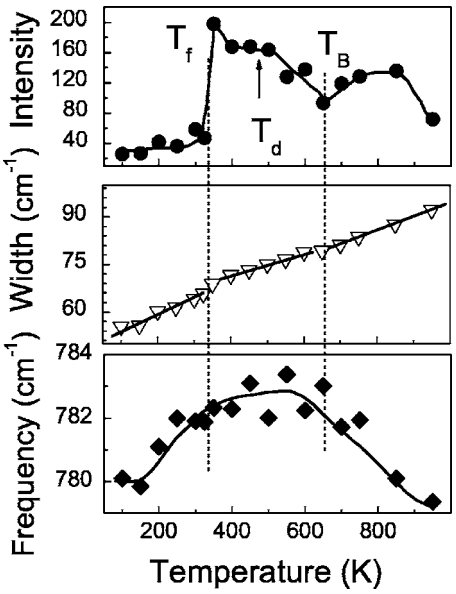

FIG. 3. Temperature dependencies of the mode intensity, width, and frequency shift around 780 cm^{-1}.

Raman spectra, respectively above and below T_f, indicate that T_f is associated with a clear structural change. It is useful to note that T_f falls well below the dielectric maximum temperature T_m and, in fact, lies where the dielectric relaxation is "exhausted;"[52] it is hereafter called the freezing temperature.

B. Characteristic temperatures around 340 K, 470 K, 650 K

The highest frequency A_{1g} mode around 780 cm^{-1} is strong and well separated from other modes, and reliable parameters can be obtained from its fitting. Figure 3 shows the temperature dependencies of its intensity, width and frequency shifts. Three ranges can clearly be identified, separated by two clear anomalies, respectively at $T_B \sim 650$ K and $T_f \sim 340$ K. In addition, a small plateau in the temperature dependence of its intensity can be noticed around an intermediate temperature $T_d \sim 470$ K. Further evidence for the existence of this intermediate temperature T_d can be found in Fig. 4, which shows the total integrated intensity in the *VV* and *VH* spectra, respectively. Upon cooling from high temperature, the *VV* intensity first decreases down to T_B, and then increases upon further cooling, with a dip around $T_d \sim 470$ K. Below T_d, the total *VV* intensity increases again and drops drastically around $T_f \sim 340$ K. It is important to note that the *VH* intensity also starts to increase below $T_d \sim 470$ K. The anomaly around 470 K must therefore reflect a significant change in the dynamical properties of PZN upon cooling. As we show below, following the model previously developed for KTN, the intermediate temperature T_d marks the onset of long-lived correlations between off-center Pb and Nb ions, i.e., local phase transitions resulting in the formation of permanent PNRs with their associated local strain fields. The large and final drop in total intensity at $T_f \sim 340$ K reveals the freezing of internal vibrational or otherwise dynamical degrees of freedom.

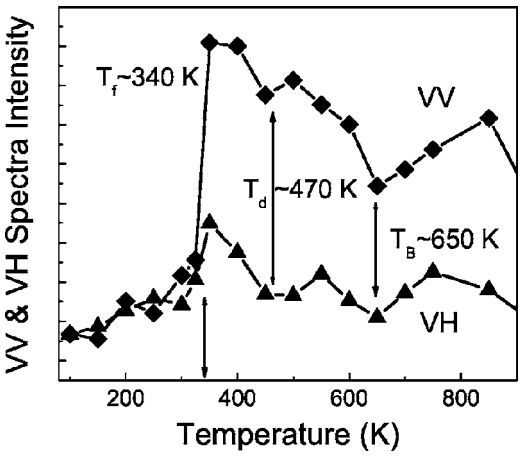

FIG. 4. Temperature dependencies of the total *VV* and *VH* spectrum intensity.

IV. PHYSICAL MODELS FOR THE LOW FREQUENCY RAMAN SPECTRUM ANALYSIS

As was seen in Fig. 1, the low frequency Raman spectra of PZN consist of a narrow central component and several broad and overlapping modes. The narrow central component or central peak (CP) is associated with slow relaxational phenomena, the characteristic time of which can be obtained from the inverse linewidth, $\tau = 2/\Delta\omega$. In addition, these spectra reveal a broad central intensity, which could be attributed either to an overdamped phonon or to a second relaxation process characterized by a shorter time. Superposed on this broad central intensity are several overlapping modes, which can couple to the central mode and/or to one another. One possibility is that of a transverse optical (TO) mode coupled to the central relaxation mode,[53,54] as proposed in several systems.[55,56] Alternatively, recent neutron scattering studies of PZN suggest a TO mode coupled to the TA(*ZB*) mode.[18,20] Such a coupling has been evidenced in normal ferroelectrics and should be active here, although one would expect it to be strongly modified by the presence of PNRs. If uncoupled, Raman modes can be modeled as damped harmonic oscillators (DHO).[31] In the following, we show that the Raman spectra can be fitted equally well by a number of different models. The validity of these models must then be judged, not so much on the quality of the fit but rather on the meaningfulness of the values obtained for the fitting parameters and of their temperature dependence.

A. One CP plus several DHOs

In the first and simplest model, we consider one narrow CP and independent DHO for all the phonons.

As usual, the CP is modeled using a Lorentzian function centered at zero frequency shift

$$\frac{2A_0}{\pi}\frac{\gamma_0}{4\omega^2+\gamma_0^2}, \tag{1}$$

where A_0 is the strength of relaxation and γ_0 is the relaxation rate. Finite frequency Raman modes can be described by DHO and the general intensity expression is then written as

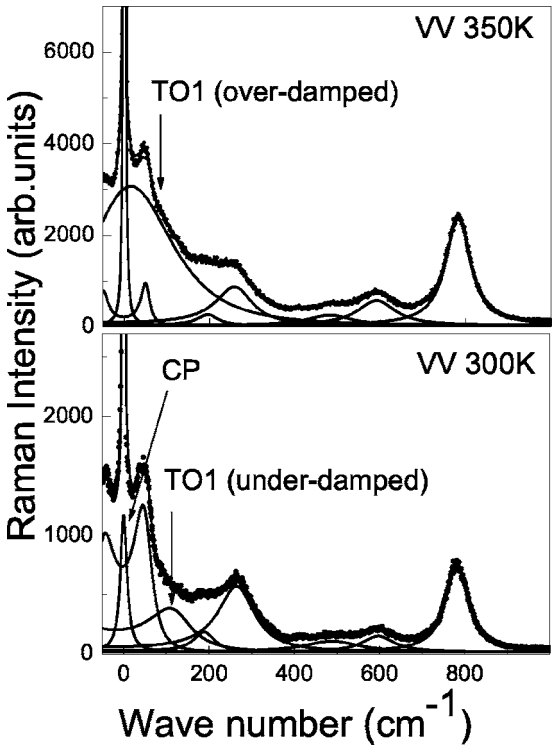

FIG. 5. Two fitting examples at 350 K and 300 K. A CP plus DHOs were used to fit the Raman spectra, see Eq. (2). The TO_1 is overdamped at 350 K and underdamped at 300 K.

$$I(\omega) = \frac{2A_0}{\pi}\frac{\gamma_0}{4\omega^2+\gamma_0^2} + \begin{pmatrix} n \\ n+1 \end{pmatrix}\sum_i \frac{A_i\Gamma_i\omega_i^2\omega}{(\omega^2-\omega_i^2)^2+\omega^2\Gamma_i^2}, \tag{2}$$

where A_i, Γ_i, and ω_i are the amplitude, damping, and frequency of the ith Raman mode. $n+1$ and n are the population factors, respectively, for the Stokes or the anti-Stokes part of the spectra, with $n=[\exp(\hbar\omega/k_BT)-1]^{-1}$. To prevent contamination of the spectra by the specularly reflected laser light, a narrow central region of ± 5 cm^{-1} was excluded in our fitting. Two examples of fits are shown in Fig. 5. The two characteristic features in this particular analysis are the narrow CP and the overdamped mode, which we associate with the soft TO_1 mode. This mode is overdamped at 350 K but underdamped at 300 K, in agreement with neutron scattering studies. Figure 6 shows the temperature dependence of the CP intensity and width. Three anomalies are apparent, around 650 K, 470 K, and 340 K. The appearance of an anomaly at an intermediate temperature, $T_d \sim 470$ K, is an essential result of the present study. It coincides with the onset of the relaxor behavior as seen in the dielectric spectra,[52] and should therefore be associated with the appearance of the PNRs and of their reorientational motion (see discussion below).

B. CP-TO coupling plus DHOs

In their neutron scattering studies, Shapiro *et al.* proposed a model in which the central component arises from a low frequency resonance in the self-energy of the soft mode.[53]

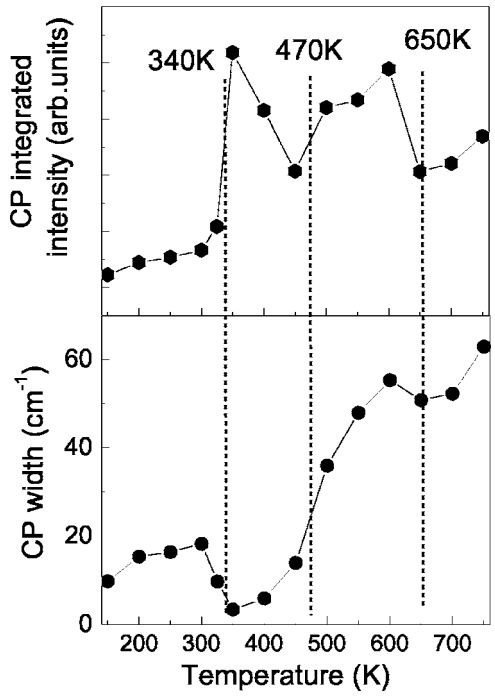

FIG. 6. Central peak intensity and width obtained by fitting Raman spectra with a Lorentzian centered at zero frequency shift and DHOs.

The spectral contribution of this mode is given in anharmonic perturbation theory as

$$S(\omega) = \frac{1}{\pi}[n+1]F\,\mathrm{Im}[\Omega^2-\omega^2+\Pi(\omega,T)]^{-1}, \tag{3}$$

where n is the phonon occupation number, Ω is the q dependent harmonic frequency, and F is the mode amplitude. In their analysis, the self-energy term $\Pi(\omega,T)$ was assumed to have the form

$$\Pi(\omega,T) = [\Delta(T) - i\omega\Gamma_0(T)] - \frac{\gamma\delta^2}{\gamma - i\omega}, \tag{4}$$

where $\Delta(T)$ is a correction to the harmonic frequency Ω due to the interaction, Γ_0 is the phonon damping, γ and δ^2 are the relaxation rate and coupling strength. Barker proposed a similar model for a two-mode coupling, starting from a set of two coupled equations of motion.[54] In our case, we considered the second mode to be the relaxation mode giving rise to the CP. With this CP-TO coupling, the dielectric constant is expressed as

$$\varepsilon(\omega) = \varepsilon(\infty) + \frac{S\omega_t^2}{\omega_t^2 - \omega^2 - c\omega_t^2/(1-i\omega\tau) - i\omega\Gamma_t}, \tag{5}$$

where $\varepsilon(\infty)$ is the high frequency dielectric constant, ω_t, Γ_t, S, c, and τ are the bare phonon mode frequency, damping, amplitude, coupling strength, and relaxation time, respectively. The spectral intensity is proportional to the imaginary part of the dielectric constant.

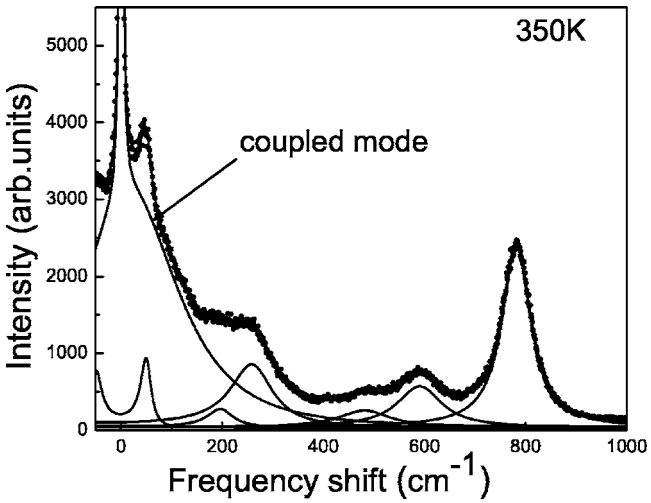

FIG. 7. A fitting example at 350 K using Barker's model, see Eq. (5).

Our Raman spectra are fitted equally well by these two different models and the values of the parameters obtained from both of them are similar. Figure 7 shows an example of a fit using Barker's model, and the parameters obtained from the two models are plotted in Fig. 8 for comparison. The parameters obtained from the two models follow identical trends, except above 650 K and in the vicinity of 470 K. With both models the CP intensity begins to increase and its width to decrease at Burns temperature, $T_B \sim 650$ K, thereafter following a similar trend to that of the total spectrum intensity (Fig. 4). With both models, the TO bare phonon frequency and damping drop at 650 K, although much more dramatically with Barker's model, increase again around 500 K and finally drop below $T_f \sim 340$ K. Below 340 K, the phonon is underdamped. These Raman results are consistent with the neutron scattering results,[17,18,20] except for the TO_1 mode frequency which is much higher in our fitting than that obtained in the neutron scattering study. As was indicated earlier, this is due to the fact that the Raman intensity in that

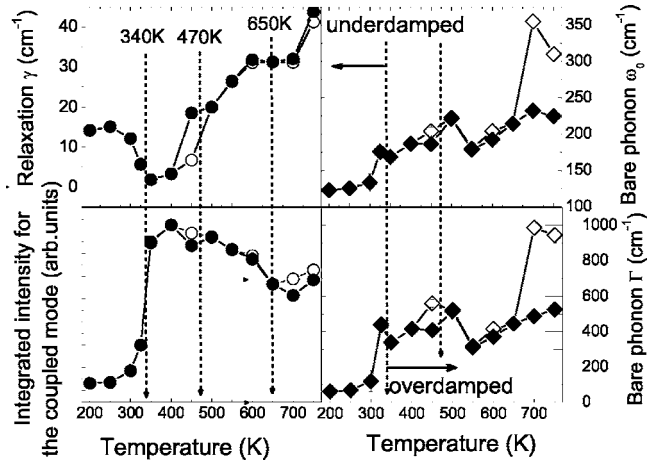

FIG. 8. Fitting parameters obtained using the Shapiro (filled symbols) and Barker's (open symbols) model; relaxation rate γ, integrated intensity of the coupled mode, bare phonon frequency ω_0 and damping Γ.

frequency range was fitted with a single peak even though two overlapping peaks appear to be present. It is worth noting that, because the TO_1 mode is strongly overdamped ($\Gamma_{TO} > \omega_{TO}$) above T_f, it could be fitted equally well by a broad CP. For the same reason, and because Shapiro's model is only the result of an anharmonic perturbation of the TO phonon, Barker's model is physically more appropriate to describe the present system. It also confirms more clearly the previously recognized changes at T_B.

C. CP plus TA-TO coupling and DHOs

A coupling between the soft TO and an acoustic TA mode has been evidenced in several normal ferroelectrics, starting with $BaTiO_3$.[57] It is therefore not surprising that such a coupling could also be active in relaxors. A TA-TO coupling was previously proposed to explain the compositional dependence of the Raman spectra of ceramic samples at room temperature,[33] although the authors only used independent oscillators in their analysis. Because of the disorder present in relaxors, we would indeed expect the mode to be coupled but we would also expect this coupling to be modified or possibly overridden by the relaxational dynamics of the PNRs. As indicated by neutron scattering,[50,51] the ~ 45 cm^{-1} frequency of the coupled TA mode corresponds to the flat wave vector range near the zone boundary, which is closest to the frequency of the zone center TO mode. Assuming that the shoulder between ~ 75 cm^{-1} and ~ 150 cm^{-1} contains contributions from both the TO and another mode or a split TO, we have fitted the spectra with a narrow CP, a TA at 50 cm^{-1} coupled to a TO mode in that frequency range and the remaining modes as DHOs. As before, the CP was fitted with a simple Lorentzian function. The spectral response in the case of a real coupling coefficient is expressed as[57]

$$S(q,\omega) = (n+1)\frac{\omega}{A^2+\omega^2 B^2}\{[(\Omega_2^2-\omega^2)B-\Gamma_2 A]F_1^2 + 2\lambda B F_1 F_2 + [(\Omega_1^2-\omega^2)B-\Gamma_1 A]F_2^2\}, \quad (6)$$

where

$$A = (\Omega_1^2-\omega^2)(\Omega_2^2-\omega^2) - \omega^2\Gamma_1\Gamma_2 - \lambda^2,$$

$$B = \Gamma_1(\Omega_2^2-\omega^2) + \Gamma_2(\Omega_1^2-\omega^2).$$

The model parameters Ω, Γ, and λ are the phonon frequency, damping, and coupling constant, while the indices 1 and 2 denote the TA and TO modes, respectively. F is the mode amplitude in Raman and the dynamic structure factor in neutron scattering. Examples of fits at two different temperatures are presented in Fig. 9. Once again, the fits are excellent. The temperature evolution of the parameters from the TA-TO coupling model are shown in Fig. 10, together with those from the earlier fitting of a CP plus DHOs for comparison. The temperature dependence of the TO parameters is almost identical for the two models as well as for the earlier Barker's model, showing a drop in both frequency and damping at 650 K, a maximum at 470 K and a final drop at ~ 340 K. However, a comparison of the CP parameters obtained with the two models reveals interesting differences

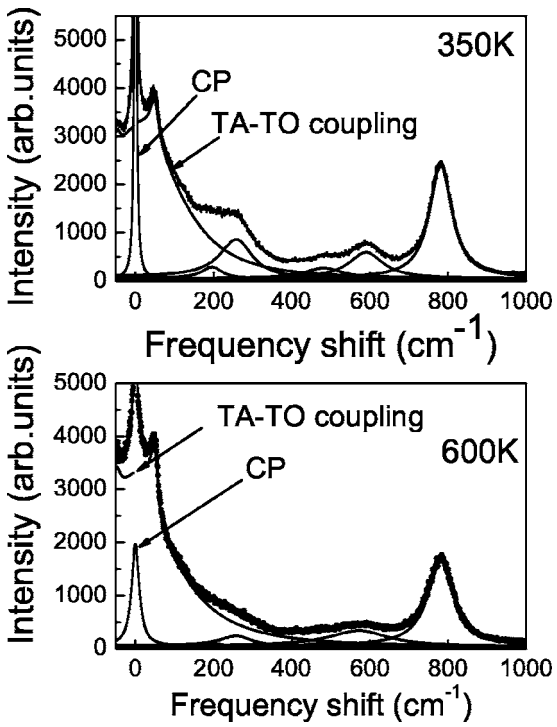

FIG. 9. Fitting spectra at 350 K and 600 K, using the CP plus coupled TA-TO model, see Eq. (6). The CP and the coupled mode are indicated by arrows.

and similarities. In particular, the two models disagree between 650 K and 470 K and below 340 K, but agree in the range 470 K–340 K, where we expect the relaxational dynamics of the PNRs to dominate. In addition, the temperature evolution of the CP intensity from the TA-TO coupling model agrees well with that from Barker's model and the total spectral intensity in Fig. 4. Figure 11 compares the temperature dependence of the coupling strength for the CP-TO from Barker's model with that from the CP+TA-TO coupling model. It is interesting to note that the TA-TO coupling coefficient is large between 650 K and 470 K and again below 340 K but small between 470 K and 340 K, while the CP-TO coupling increases in this latter range.

V. DISCUSSION

Based on the fitting results presented above, it is clear that the goodness of fit is not a sufficient criterion to validate a particular model. A critical examination of the values of the fitted parameters and of their temperature dependence is also essential. In addition, the comparison of the fitted parameters from different models can help identify the model-independent characteristics of the system studied and shed light on the particular physics of that system, here the formation and dynamics of polar nanoregions and their possible coupling to phonons in PZN. Following this approach, we first note that a common feature of the results obtained from the different models is the existence of three characteristic temperatures, T_B, T_f, and an intermediate temperature T_d, or equivalently four characteristic temperature ranges. In the following discussion we first show that the similarities and

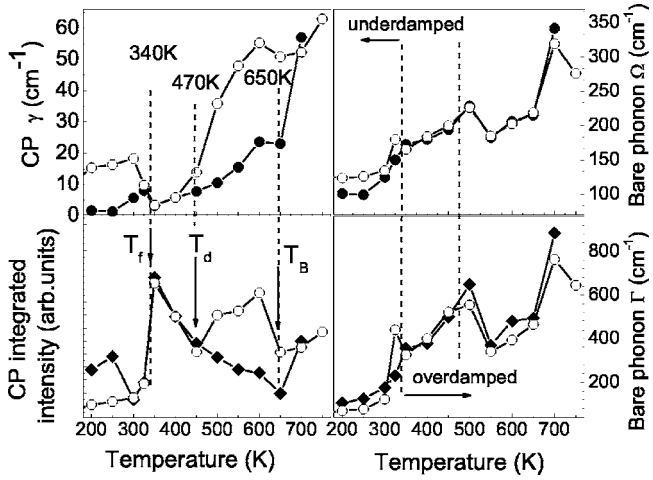

FIG. 10. Results of CP+TA-TO coupling (filled symbols), and of a single CP plus DHOs (open symbols).

differences between these results can be analyzed within the framework of these four characteristic temperature ranges (see Figs. 8, 10, and 11). Then, we discuss the meaning of the four characteristic temperatures identified. In particular, the identification of an intermediate temperature, T_d, not only raises the question of the significance of this temperature but also, by consequence, that of Burns temperature, commonly associated with the appearance of the PNRs.

Particularly revealing illustrations of the first point can be found in the summary Fig. 12, in which we plot the integrated intensities and widths of the CP obtained from the four models. Between T_B and T_d, the CP-TO and the CP+DHOs models are seen to put equal intensities in the CP and significantly more than does the CP+TA-TO model. This observation means that the CP-TO coupling does not significantly affect the intensity distribution between the two individual components, CP and TO, and suggests that the relaxation giving rise to the CP is not strongly coupled to the

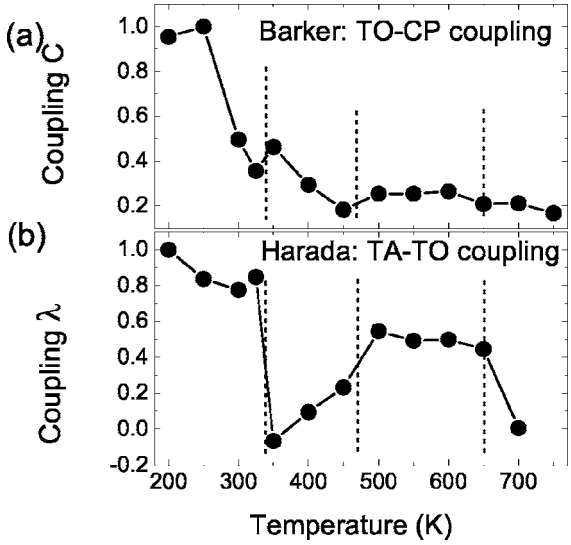

FIG. 11. Temperature dependences of the relative coupling strength for two models; (a) CP-TO coupling; (b) CP plus TA-TO coupling.

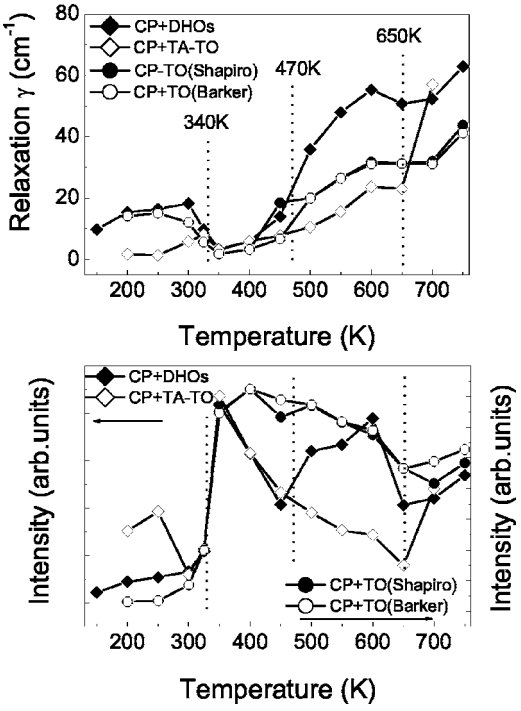

FIG. 12. Comparison of the CP integrated intensities and widths obtained from the four models.

TO phonon mode between T_B and T_d. In this range, the narrow CP must therefore be due to an independent relaxation process, the rate of which is given by γ and decreases from approximately 750 GHz down to 250 GHz across the range. In the same range, our Raman results suggest and neutron scattering results confirm[50] that the TO mode is strongly overdamped below T_B and therefore sufficiently broad so as to overlap significantly with the flat zone boundary TA mode. This is the temperature region in which the TO has all but disappeared from the neutron scattering spectra ("waterfall" phenomenon) and a ridge of scattering at constant Q suggests an almost vertical drop of the TO branch down into the TA branch.[50] Therefore, in Fig. 12, the CP+TA-TO model provides the more physically plausible results. It shows the CP intensity or strength of the relaxation increasing to a certain level and then saturating around 500 K. In PZN as in many simple perovskite ferroelectrics such as $BaTiO_3$, the TA-TO coupling is expected to be active, probably even enhanced by the disorder in PZN. This appears to be further confirmed in Fig. 11, where the TA-TO coupling coefficient is seen to be quite strong between T_B and T_d, while the CP-TO coupling is much weaker. We further discuss the specifics of this TA-TO coupling later in this section.

In the next lower temperature range, between T_d and T_f, the fact that both the CP+TA-TO and the CP+DHOs models put equal intensities in the CP indicates that the TA-TO coupling does not influence the CP; the same results are obtained for the CP, whether the phonons are treated as coupled or uncoupled. The higher CP intensity obtained from the CP-TO model is due to the fact that this model tends to emphasize the very low frequency spectral region. However, since the TO had already become decoupled from the CP slower dynamical process in the previous higher temperature range, we do not expect this coupling to play an important role in this lower temperature range either. The temperature evolution of the CP in this lower range is therefore most likely that given by either of the two superposed lower curves in Fig. 12, obtained from the CP+DHOs or CP+TA-TO model. In this temperature range, the CP intensity is seen to increase more rapidly than in the previous higher temperature range and all four models give approximately the same low relaxation rate γ. These observations all converge to suggest that the CP dynamics in this range is dominated by the reorientation of the PNRs, whose relaxor behavior also dominates the dielectric spectrum. This interpretation is further confirmed in our Raman data by the increase in the total VH intensity shown in Fig. 4, indicative of rotations. However, the same changes that are responsible for the evolution of the CP also appear to influence the TA-TO coupling, the coefficient of which goes through a minimum in Fig. 11. Overall, from the considerations presented in this and the previous section, the CP+TA-TO model appears to yield the more physically plausible results.

The physical insight that we can gain from the fit results for the bare TO phonon should be somewhat more speculative since the spectral region from 75 cm^{-1} to 150 cm^{-1} was fitted with a single peak. However, the fact that all models yield similar trends for the bare TO phonon adds credence to the results obtained. Moreover, as we shall see, the trends observed here support the interpretations obtained from the CP and even provide complementary information. Over the whole temperature range investigated, both the frequency and damping of the bare phonon exhibit a decreasing trend. The overall decrease in frequency can be attributed to its soft character and the decrease in damping to an increasingly static order. At approximetely 500 K, all models show a sudden increase in both frequency and damping of the bare TO phonon. Since these parameters are those of the bare phonon, the increase in frequency cannot be attributed to coupling but could be due to a change in crystalline environment and the accompanying change in force constants. We will demonstrate later that 500 K or thereabout (470 K) marks the onset of a series of local phase transitions ending at the "freezing" temperature T_f. However, we would not expect that these would lead to an increase in damping of the bare phonon. The observed increase may instead reflect a static broadening of the spectral features in this temperature range due to the appearance of local strain fields resulting from the local phase transitions. It would therefore be more accurate to refer to the width of the bare phonon rather than to its damping. The final drop in frequency and width of the bare phonon at T_f also corresponds to a sudden intensity drop in the 75 cm^{-1} to 150 cm^{-1} frequency range and is therefore less reliable. It is possibly due to the disappearance of the additional peak in that range, leaving a TO mode with its true frequency. This would seem to be confirmed by the fact that the TO frequency thus obtained is comparable to that obtained from neutron scattering.

We now turn to the second point mentioned at the beginning of this discussion, relative to the meaning of the three temperatures, T_B, T_d, and T_f, a meaning already alluded to in the previous section. Because it is an important result of the present study, we shall start with a discussion of the interme-

diate temperature. Although it may not have been recognized as such, the intermediate temperature T_d has been apparent for some time in a number of published experimental results. First and foremost, this is the temperature at which the real part of the dielectric constant begins to exhibit a strong frequency dependence and an imaginary part appears,[52] as expected from the Kramers-Kronig relationships, and electrostrictive resonances are observed in the dielectric spectrum.[58,59] It is also the temperature at which the elastic neutron diffuse scattering begins to grow around specific reciprocal lattice points and in certain directions and the Bragg peak intensities in the [100] and [111] directions also begin to increase.[19,60,61] The former observation confirms very definitely the onset of local phase transformations and the latter the appearance of strain fields (relief of extinction). To better understand the nature of these local phase transformations, we refer to KTN and PMN. In KTN, dynamic correlations of the off-center Nb displacements are observed at higher temperature, with the Ta ions remaining on center. At a lower temperature, which corresponds to the intermediate temperature T_d at which the relaxor behavior becomes apparent, extended x-ray-absorption fine structure (EXAFS) results[14] indicate that the Ta ions also become displaced from their high symmetry site and the Raman spectra exhibit sharp first-order features,[62] indicating a lowering of the local symmetry or a local phase transition. Also, the broad Raman peak in the 500 cm^{-1} to 600 cm^{-1} range of the PMN spectrum splits and exhibits an order parameter behavior below this intermediate temperature. By analogy, we therefore identify T_d in PZN as the temperature at which local phase transitions begin to take place. Because these are local (x-rays do not reveal any change in macroscopic symmetry), they generate local strain fields. T_d can therefore be said to be the temperature at which the PNRs appear, where we associate PNRs with long-lived or permanent correlations between atomic displacements of not only the off-center Pb and Nb ions but possibly also of other initially on-center ions. It is also interesting to note that Brillouin scattering measurements in PZN[36] show a hysteresis precisely between T_d and T_f, suggesting that the local phase transitions are first-order-like.

The above interpretation of the intermediate temperature T_d suggests that correlations at higher temperature are only dynamic or short lived, and only between intrinsically off-center ions (Pb and Nb) and, most importantly, without the presence of local strain fields. The meaning of Burns temperature can then be inferred from a combination of our Raman results and the neutron scattering results of Gehring *et al.*[50] Our Raman spectra reveal a sharp drop in the width of the CP (i.e., the relaxation rate) and an increase in intensity upon cooling through T_B. The latter is even more clearly seen on the raw spectra than in the integrated intensity of the CP. Concurrently, the neutron scattering results reveal the disappearance of the zone center TO phonon from the inelastic spectra, which suggests a very high damping. A natural explanation of both these observations is that T_B is the temperature at which the growing lifetime of the dynamic correlations between off-center ions exceeds the inverse frequency of the TO phonon. This explanation is supported by high resolution pulsed neutron measurements of the atomic pair-density function (PDF) that have suggested that the local Pb polarization is dynamically correlated below T_B.[63] Above T_B, the local intersite motion of the off-center ions is fast and uncorrelated, dynamically broadening the TO phonon. Below T_B, these correlations, though still dynamic in the absolute (absence of local strain fields), will appear static to the TO phonon whose frequency will then increase, as observed below 500 K. It is then likely that the cooperative intersite motion of the Pb ions will not be able to follow the TO phonon, which should thence not become overdamped, contrary to experimental results. The solution to this apparent conflict may come from the recognition that the off-center Nb ions are still able to tunnel locally between their equivalent sites and therefore follow the TO phonon, but their motion is now correlated. As described in the microscopic model below, the number of equivalent sites available to the off-center Nb ions will be restricted by the now correlated Pb ions, which may result in a more cooperative motion of the off-center Nb ions themselves and an overdamped TO phonon. In addition, because the correlations between Pb ions will now be static on the time scale of the TO phonon, they will break the symmetry seen by the TO phonon and significantly enhance its coupling to the TA phonon, as indicated in Fig. 11 by the increase in the TA-TO coupling coefficient. Last but not least, this explains the initial observation by Burns[64] of a deviation of the refractive index from a linear temperature dependence at T_B. It is important to note that such a deviation does not indicate the onset of birefringence, which in fact has been shown by Ye *et al.* to occur in PZN close to our intermediate temperature T_d.[38] Instead, the faster-than-linear decrease in the refractive index with temperature observed by Burns is quite consistent with the loss of polarizability resulting from correlated off-center Pb ions that can no longer follow the TO mode.

The third and lowest temperature, T_f, is marked by a drop in the intensity of the CP, a minimum of its width and a drop of both the bare phonon frequency and width. As seen in Fig. 4, the overall spectral intensity also drops at that point, suggesting the "freezing" of vibrational or otherwise dynamical degrees of freedom. The drop in intensity of the CP and the minimum in its width suggests the progressive arrest of the relaxational motion taking place at higher temperature, primarily the rotation of the PNRs. This interpretation is confirmed by the fact that T_f is also the temperature at which the frequency dispersion of the dielectric constant vanishes[52] and the TO phonon reappears in the inelastic neutron scattering spectra. The drop in frequency of the bare TO phonon is more difficult to explain but also less reliable, given our fitting with a single peak in this part of the spectrum and the very large spectral changes taking place at that temperature. It may simply reflect the disappearance of the "other" spectral component overlapping with the TO.

Although the present Raman results by themselves do not permit a detailed description of the atomic motion underlying this evolution, one can nevertheless attempt such a description by referring to structural measurements of PZN and our extensive understanding of KTN (see Ref. 31 and references therein). In KTN, the slow dynamics or relaxor behavior is due to the correlated motion of the off-center niobium ions. These are displaced in a $\langle 111 \rangle$ direction and each one can tunnel between several equivalent or symmetry-related

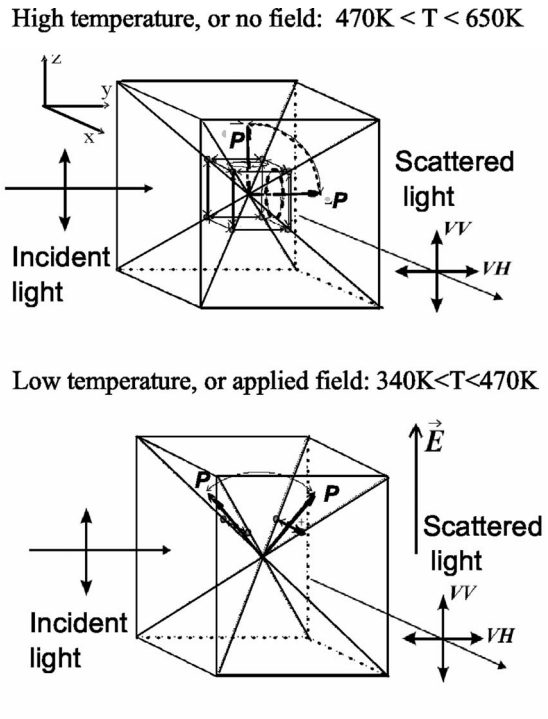

FIG. 13. A schematic description of the Nb ion motion and its effect on the *VV* and *VH* spectrum intensity: two-time scales. The Pb ion motion between its equivalent symmetry-related sites, although not shown in the figure, can be described in a similar way.

sites (fast motion). At high temperatures, eight sites are available within the unit cell and the niobium ions can follow the TO motion.[65] Starting at a Burns-like temperature, $T_B \sim T_d + 25-30$ K, correlations develop between niobium ions and the dielectric constant departs from a Curie-Weiss behavior. Experimental results obtained in KTN have led to the following model:[66] near T_d, the onset of local phase transitions (similar to those observed at higher Nb concentrations, only local at low Nb concentrations) progressively restricts the motion of the off-center niobium ions first to four, then two sites, and finally to a single site. The restriction of the Nb ions to four sites results in a $\langle 100 \rangle$ time-averaged dipole moment (local tetragonal symmetry) with possible rotation of the tetragonal axis (slow motion). Similarly, the restriction to two sites results in a $\langle 110 \rangle$ time-averaged dipole moment (local orthorhombic symmetry), with possible rotation of the orthorhombic axis. This model is represented graphically in Fig. 13. It has led us to describe the dynamics in KTN in terms of two time scales, the fast intersite tunneling motion of individual Nb ions and the slow motion of their time-averaged dipole moment, recently confirmed by NMR measurements.[67] In PZN (and PMN) both the lead and niobium ions have now been shown to be off-center,[5,6,12,13] each with a number of equivalent or symmetry-related sites, and a similar model can be proposed. Above T_B, Pb and Nb ions can reorient freely between several of these sites and their motion is sufficiently fast that they can follow the TO mode. There is no relaxation motion and accordingly only a small narrow CP if any but a very broad central intensity. Because of a heavier mass, the Pb motion between sites is likely to be thermally activated while the Nb motion takes place through tunneling. Between T_B and T_d, the local displacements of the Pb ions become correlated and they can no longer follow the TO mode, contrary to the Nb ions, which continue to tunnel locally. In fact, the overdamping of the TO phonon starting at T_B suggests a particularly strong coupling to the cooperative niobium motion, a point worth studying further. Permanent PNRs with associated local strain fields form at T_d or, equivalently, local phase transformations begin to occur. It is interesting to note that, above T_d, the absence of local strain fields and associated effects means that the characteristic frequency of the relaxational dynamics falls between the respective frequencies of the TA and TO mode while, below T_d, it falls below both TO and TA frequencies. One would therefore expect to observe a change in the TA-TO mode coupling at T_d, and in fact the TA-TO coupling coefficient is seen to drop below T_d. Continuing with the proposed model below T_f, both Pb and Nb ions within a PNR are displaced in the same $\langle 111 \rangle$ direction, i.e., they are both restricted to a fixed site within the unit cell and the fast Nb motion has all but ceased. This can explain why the TO mode is no longer overdamped and reappears in the neutron spectra. Although the fast tunneling motion of the niobium ions has all but ceased below T_f, rotation of the local rhombohedral axis should still be possible in principle. However, an already much slower reorientation of the PNRs at low temperatures and the resulting stronger time-averaged local random fields may in fact lead to the freezing of the slow motion as well, explaining the drastic loss of Raman intensity and abrupt changes in the Raman spectra. If the correlations of the lead displacements should clearly affect the number of equivalent sites allowed to the Nb off-center ions, an interesting and as yet unanswered question concerns the possible effect of the intersite tunneling motion of the Nb ions on the Pb dynamics.

VI. SUMMARY AND CONCLUSIONS

The polarized Raman spectra of a PZN single crystal have been measured over a wide temperature range and analyzed using different models. An important result of this work is the realization that excellent fits of the spectra can be obtained from all the models used. It is only by comparing the temperature dependence of the fitting parameters that the most physically meaningful model can be selected. The comparative examination of the fitting results obtained from the different models confirms the existence of an intermediate temperature T_d, between Burns temperature T_B, and the freezing temperature T_f. In view of the confirmation of the existence of this intermediate temperature, we have reexamined the meaning of Burns temperature. Our Raman results suggest that it is the temperature at which the lifetime of the dynamic correlations between the off-center Pb ions exceeds the period of the TO phonon, then appearing static on the time scale of the phonon (or *quasidynamic* on an absolute time scale). This crossover from fully dynamic to quasidynamic is marked by a narrowing-down of the low frequency features of the Raman spectrum, the disappearance of the long wavelength TO phonon from the inelastic neutron scat-

tering spectrum as well as a faster-than-linear decrease with temperature of the refractive index. Between T_B and the intermediate temperature T_d, the dynamics is dominated by the TA-TO coupling enhanced by the quasidynamic correlations between off-center ions. Next, T_d marks the onset of local phase transitions, or the appearance of static or permanent correlations of the off-center ion displacements as well as the off-centering of other previously on-center ions. This is really the temperature at which the PNRs can be said to form, with their accompanying local strain fields giving rise to a steep increase in elastic diffuse neutron scattering. Also at that temperature, the dielectric constant begins to exhibit the strong frequency dispersion that is the hallmark of relaxors. The temperature range between T_d and the freezing temperature T_f is characterized in the Raman spectra by the growth of the *VH* component of scattering, an increase in intensity and decrease in width of the central peak, and increases in both the frequency and width of the bare TO phonon. It is dominated by the rotation of the PNRs and can appropriately be designated as *a quasistatic stage*. It is interesting to note that the temperature range in which the dielectric constant goes through its maxima lies precisely in this range between T_d and T_f. The lowest and final temperature, T_f, is marked by a drastic overall drop in scattered intensity and abrupt changes in the Raman spectrum, which strongly suggest an arrest of the low frequency relaxational motion. It is also the temperature at which the frequency dependence disappears in the dielectric constant and an underdamped TO phonon reappears in the neutron scattering spectrum. Below T_f, the dynamics appears to be dominated by a renormalized TA-TO coupling induced by static disorder. Based on the above interpretation of the Raman results, one can therefore identify four main temperature ranges or stages in the evolution of the polarization of PZN: *a fully dynamic stage* above T_B, *a quasidynamic stage* between T_B and T_d, *a quasistatic stage* between T_d and T_f and *a static stage* below T_f.

From a comparison of PZN with KTN, we have also proposed a microscopic physical description of the local dynamics taking place in PZN between T_d and T_f. The fast tunneling motion of Nb ions would coexist with the slow thermally activated and cooperative motion of the Pb ions that constitutes the basic mechanism for the reorientation of the PNRs. Restrictions placed by the Pb ions on the number of allowed symmetry-related sites available to the Nb ions should make their fast motion more cooperative, thereby explaining the overdamping of the TO phonon. When this fast motion ceases below T_f, an underdamped TO phonon reappears in the neutron scattering spectra.

ACKNOWLEDGMENTS

This work was supported by grants from the U.S. Department of Energy, Grant No. DE-FG02-00ER45842 (Lehigh), and the Office of Naval Research, Grant No. N00014-99-1-0738 (Simon Fraser).

*Electronic address: jt02@lehigh.edu
†Present address: Department of Geosciences, Princeton University, Princeton, NJ 08544, USA.
‡Present address: National High Magnetic Field Laboratory, Florida State University, Tallahassee, FL 32310, USA.

[1] L. E. Cross, Ferroelectrics **76**, 241 (1987).
[2] Z.-G. Ye, Key Eng. Mater. **155-156**, 81 (1998).
[3] S.-E. Park and T. R. Shrout, J. Appl. Phys. **82**, 1804 (1997).
[4] H. Fu and R. E. Cohen, Nature (London) **403**, 281 (2000).
[5] I. W. Chen, P. Li, and Y. Wang, J. Phys. Chem. Solids **57**, 1525 (1996).
[6] I. W. Chen, J. Phys. Chem. Solids **61**, 197 (2000).
[7] P. K. Davies and M. A. Akbas, J. Phys. Chem. Solids **61**, 159 (2000).
[8] P. Bonneau, P. Garnier, G. Calvarin, E. Husson, J. R. Gavarri, and A. Morell, J. Solid State Chem. **91**, 350 (1994).
[9] S. Vakhrushev, S. Zhukov, G. Fetisov, and V. Chernyshov, J. Phys.: Condens. Matter **6**, 4021 (1994).
[10] R. Blinc, A. Gregorovic, B. Zalar, R. Pirc, V. V. Laguta, and M. D. Glinchuk, Phys. Rev. B **63**, 024104 (2000).
[11] K. Fujishiro, T. Iwase, Y. Uesu, Y. Yamada, B. Dkhil, J.-M. Kiat, S. Mori, and N. Yamamoto, J. Phys. Soc. Jpn. **69**, 2331 (2000).
[12] E. Prouzet, E. Husson, N. de Mathan, and A. Morell, J. Phys.: Condens. Matter **5**, 4889 (1993).
[13] V. A. Shuvaeva, I. Pirog, Y. Azuma, K. Yagi, K. Sakaue, H. Terauchi, I. P. Raevskii, K. Zhuchkov, and M. Yu Antipin, J. Phys.: Condens. Matter **15**, 2413 (2003).
[14] O. Hanske-Petitpierre, Y. Yacoby, J. Mustre de Leon, E. A. Stern, and J. J. Rehr, Phys. Rev. B **44**, 6700 (1991).
[15] Y. Yan, S. J. Pennycook, Z. Xu, and D. Viehland, Appl. Phys. Lett. **24**, 3145 (1998).
[16] V. Gosula, A. Tkachuk, K. Chung, and H. Chen, J. Phys. Chem. Solids **61**, 221 (2000).
[17] P. M. Gehring, S. E. Park, and G. Shirane, Phys. Rev. Lett. **84**, 5216 (2000).
[18] S. Wakimoto, C. Stock, Z.-G. Ye, W. Chen, P. M. Gehring, and G. Shirane, Phys. Rev. B **66**, 224102 (2002).
[19] D. La-Orauttapong, J. Toulouse, J. L. Robertson, and Z.-G. Ye, Phys. Rev. B **64**, 212101 (2001).
[20] J. Hlinka, S. Kamba, J. Petzelt, J. Kulda, C. A. Randall, and S. J. Zhang, Phys. Rev. Lett. **91**, 107602 (2003).
[21] K. Ohwata, K. Hirota, P. W. Rehrig, Y. Fujii, and G. Shirane, Phys. Rev. B **67**, 094111 (2003).
[22] D. La-Orauttapong, J. Toulouse, Z.-G. Ye, W. Chen, R. Erwin, and J. L. Roberston, Phys. Rev. B **67**, 134110 (2003).
[23] Y. Bing, A. A. Bokov, Z.-G. Ye, B. Noheda, and G. Shirane, J. Phys.: Condens. Matter **17**, 2493 (2005).
[24] D. Viehland, S. Jang, and L. E. Cross, J. Appl. Phys. **68**, 2916 (1990).
[25] A. K. Tagantsev and A. E. Glazounov, Phys. Rev. B **57**, 18 (1998).
[26] Z.-Y. Cheng, R. S. Katiyar, X. Yao, and A. S. Bhalla, Phys. Rev. B **57**, 8166 (1998).
[27] A. A. Bokov and Z.-G. Ye, Phys. Rev. B **66**, 064103 (2002).

[28] I. Siny, S. Lushnikov, R. Katiyar, and V. Schmidt, Ferroelectrics **226**, 191 (1990).
[29] I. Siny, S. G. Lushnikov, R. S. Katiyar, and E. A. Rogacheva, Phys. Rev. B **56**, 7962 (1997).
[30] F. Jiang, S. Kojima, C. Zhao, and C. Feng, J. Appl. Phys. **88**, 3608 (2000).
[31] O. Svitelskiy, J. Toulouse, G. Yong, and Z.-G. Ye, Phys. Rev. B **68**, 104107 (2003).
[32] J. Kreisel, B. Dkhil, P. Bouvier, and J.-M. Kiat, Phys. Rev. B **65**, 172101 (2002).
[33] I. Dujovne, T.-Y. Koo, A. Pinczuk, S.-W. Cheong, and B. S. Dennis, Phys. Rev. B **66**, 064110 (2002).
[34] F. M. Jiang and S. Kojima, Phys. Rev. B **62**, 8572 (2000).
[35] M. H. Kuok, S. C. Ng, N. Yasuda, H. Ohwa, H. Orihara, and Y. Ishibashi, Solid State Commun. **118**, 169 (2001).
[36] Y. Gorouya, Y. Tsujimi, M. Iwata, and T. Yagi, Appl. Phys. Lett. **83**, 1358 (2003).
[37] J. Toulouse, D. La-Orauttapong, and O. Svitelskiy, Ferroelectrics **302**, 271 (2004).
[38] Z.-G. Ye, M. Dong, and L. Zhang, Ferroelectrics **229**, 223 (1999).
[39] J. Chen, H. M. Chan, and M. P. Harmer, J. Am. Ceram. Soc. **72**, 593 (1989).
[40] C. A. Randall and A. S. Bhalla, Jpn. J. Appl. Phys., Part 1 **29**, 327 (1990).
[41] A. D. Hilton, D. J. Barber, C. A. Randall, and T. R. Shrout, J. Mater. Sci. **29**, 3462 (1990).
[42] T. Egami, W. Dmowski, S. Teslic, P. K. Davies, I.-W. Chen, and H. Chen, Ferroelectrics **206/207**, 231 (1998).
[43] V. Gosula, A. Tkachuk, K. Chung, and H. Chen, J. Phys. Chem. Solids **61**, 221 (2000).
[44] D. M. Fanning, I. K. Robinson, S. T. Jung, E. Colla, D. D. Viehland, and D. A. Payne, J. Appl. Phys. **87**, 840 (2000).
[45] D. M. Fanning, I. K. Robinson, X. Lu, and D. A. Payne, J. Phys. Chem. Solids **61**, 209 (2000).
[46] Z. Xu, S. M. Gupta, D. Viehland, Y. Yan, and S. J. Pennycook, J. Am. Ceram. Soc. **83**, 181 (2000).
[47] F. Jiang, S. Kojima, C. Zhao, and C. Feng, Appl. Phys. Lett. **79**, 3938 (2001).
[48] E. Salje and U. Bismayer, J. Phys.: Condens. Matter **1**, 6967 (1989).
[49] U. Bismayer, V. Devarajan, and P. Groves, J. Phys.: Condens. Matter **1**, 6977 (1989).
[50] P. M. Gehring, S. E. Park, and G. Shirane, Phys. Rev. B **63**, 224109 (2001).
[51] D. La-Orauttapong, Ph.D thesis, Lehigh University, 2003.
[52] M. L. Mulvihill, S. E. Park, G. Risch, Z. Li, and K. Uchino, Jpn. J. Appl. Phys., Part 1 **35**, 3984 (1996).
[53] S. M. Shapiro, J. D. Axe, G. Shirane, and T. Riste, Phys. Rev. B **6**, 4332 (1972).
[54] A. S. Barker, Jr., Phys. Rev. B **12**, 4071 (1976).
[55] M. Hafid, G. E. Kugel, A. Kania, K. Rolede, and M. D. Fontana, J. Phys.: Condens. Matter **4**, 2333 (1992).
[56] W. Fortin, G. E. Kugel, J. Grigas, and A. Kania, J. Appl. Phys. **79**, 4273 (1996).
[57] J. Harada, J. D. Axe, and G. Shirane, Phys. Rev. B **4**, 155 (1971).
[58] R. Pattnaik and J. Toulouse, Phys. Rev. Lett. **79**, 4677 (1997).
[59] Z.-Y. Cheng, R. S. Katiyar, X. Yao, and A. S. Bhalla, Phys. Rev. B **57**, 8166 (1998).
[60] D. La-Orauttapong, J. Toulouse, Z.-G. Ye, R. Erwin, J. L. Robertson, and W. Chen, in *Fundamental Physics of Ferroelectrics 2002*, edited by R. E. Cohen, AIP Conf. Proc. No. 99 (AIP, New York, 2002).
[61] T. Iwase, H. Tazawa, K. Fujishiro, Y. Uesu, and Y. Yamada, J. Phys. Chem. Solids **60**, 1419 (1999).
[62] D. M. Larsen, Phys. Rev. B **44**, 5629 (1991).
[63] T. Egami, W. Dmowski, and E. Mamontov, *Fundamental Physics of Ferroelectrics* (Williamsburg, VA, 2003).
[64] G. Burns and F. H. Dacol, Solid State Commun. **48**, 853 (1983).
[65] J. P. Sokoloff, L. L. Chase, and L. A. Boatner, Phys. Rev. B **41**, 2398 (1990).
[66] L. A. Knauss, X. M. Wang, and J. Toulouse, Phys. Rev. B **52**, 13261 (1995).
[67] S. Rankel, B. Zalar, V. V. Laguta, R. Blinc, and J. Toulouse, Phys. Rev. B **71**, 144110 (2005).